

Charge doping versus disorder in CeFeAsO: do the in- and out-of-plane dilutions play the same role?

G. Prando,^{1,*} O. Vakaliuk,¹ S. Sanna,² G. Lamura,³ T. Shiroka,^{4,5} P. Bonfà,⁶
 P. Carretta,² R. De Renzi,⁶ H.-H. Klauss,⁷ S. Wurmehl,¹ C. Hess,¹ and B. Büchner^{1,7}
¹*Leibniz-Institut für Festkörper- und Werkstofforschung (IFW) Dresden, D-01171 Dresden, Germany*
²*Dipartimento di Fisica and Unità CNISM di Pavia, Università di Pavia, I-27100 Pavia, Italy*
³*CNR-SPIN and Università di Genova, I-16146 Genova, Italy*
⁴*Laboratorium für Festkörperphysik, ETH-Hönggerberg, CH-8093 Zürich, Switzerland*
⁵*Paul Scherrer Institut, CH-5232 Villigen PSI, Switzerland*
⁶*Dipartimento di Fisica and Unità CNISM di Parma, Università di Parma, I-43124 Parma, Italy*
⁷*Institut für Festkörperphysik, Technische Universität Dresden, D-01062 Dresden, Germany*
 (Dated: May 29, 2022)

We provide direct experimental evidence for the identical effect of the in-plane $\text{Fe}_{1-x}\text{Co}_x$ and of the out-of-plane O_{1-x}F_x chemical dilutions on the itinerant spin-density-wave (SDW) magnetic phase in CeFeAsO. Remarkably, the suppression of SDW is not sensitive at all to the different kinds of disorder introduced in the two cases. Still, it is clearly shown that the sizeable in-plane disorder induced by the $\text{Fe}_{1-x}\text{Co}_x$ substitution is highly effective in suppressing T_c . Differently from what is observed in $\text{CeFeAsO}_{1-x}\text{F}_x$, the ordered magnetic phase of the Ce sublattice is preserved throughout the whole phase diagram in $\text{CeFe}_{1-x}\text{Co}_x\text{AsO}$ ($x \leq 0.2$). An intriguing effect is encountered, whereby the magnetic coupling among Ce^{3+} ions is enhanced by the superconducting phase.

PACS numbers: 74.70.Xa, 74.25.Dw, 74.25.Ha, 76.75.+i

The substitution of $\sim 10\%$ of O^{2-} ions by F^- leads to the emergence of high- T_c superconductivity (SC) in LaFeAsO [1, 2] and in other oxy-pnictides [3–6]. Although such chemical dilution is realized out of the FeAs layers, it is known to induce a charge doping in the Fe bands. This strategy allows one to reach $T_c \simeq 55$ K in $\text{SmFeAsO}_{1-x}\text{F}_x$, namely one of the highest values among all the Fe-based SC [7–10]. In spite of the lower T_c values, also other kinds of chemical substitutions which still give rise to SC in Fe-based materials are widely studied. These involve the dilution of transition metal (TM) elements on the FeAs layers [11, 12], the most common one being probably cobalt [13–18]. Whether the chemical substitution of Fe by other TM elements effectively induces a charge doping similarly to the case of O_{1-x}F_x has been subject of recent intense efforts on both the computational and the experimental sides, particularly in the case of $\text{Fe}_{1-x}\text{Co}_x$. Contrasting results have been reported from density-functional theory (DFT) calculations [19, 20] as well as from measurements via x-rays absorption [21, 22] and photoemission [23] spectroscopies. Moreover, the perturbation induced by the $\text{Fe}_{1-x}\text{TM}_x$ substitution is expected to introduce a high degree of in-plane disorder, in turn destabilizing the magnetic itinerant spin-density-wave (SDW) phase [19, 24]. This is consistent with data for different TM elements in 122, where a common scaling for the suppression of SDW is realized by considering the amount of dilution rather than the effective charge doping [11]. Such picture clearly goes far beyond the scenario of the weakening of the Fermi-surface nesting induced by charge doping [25]. The interplay of the effects of such disorder on the itinerant

magnetic phase and SC is even reported to lead to a counterintuitive enhancement of T_c with increasing the degree of disorder in the underdoped region of the phase diagram [26].

In this Letter we provide direct evidence for the equivalence of the in-plane $\text{Fe}_{1-x}\text{Co}_x$ and out-of-plane O_{1-x}F_x chemical dilutions in CeFeAsO as far as the magnetic properties are concerned. Measurements of muon-spin spectroscopy ($\mu^+\text{SR}$) show how both these substitutions lead to a *quantitatively identical* suppression of the SDW phase as a function of x . Two different regimes are detected and a short-range magnetic phase is found to nanoscopically coexist with SC within a narrow range of x values. Remarkably, the SDW transition temperature T_N is not affected at all by the degree of the in-plane disorder. However, the in-plane disorder itself strongly affects the properties of SC, T_c being sizeably suppressed by the $\text{Fe}_{1-x}\text{Co}_x$ dilution with respect to what is realized via the O_{1-x}F_x substitution. The magnetic ordering temperature T_N^{Ce} for the Ce sublattice is preserved throughout the whole phase diagram in $\text{CeFe}_{1-x}\text{Co}_x\text{AsO}$ independently from the SDW phase, at variance with what is reported for $\text{CeFeAsO}_{1-x}\text{F}_x$ [6, 10]. Finally, an intriguing correlation among the dome-like features of the phase diagram for both T_c and T_N^{Ce} is described suggesting an enhancement of the magnetic coupling among Ce^{3+} ions mediated by the SC phase.

Powder samples of $\text{CeFe}_{1-x}\text{Co}_x\text{AsO}$ ($0 \leq x \leq 0.2$) were synthesized as described in detail in the supplemental material (SM). The characterization of the samples was performed using electrical transport [27] and dc magnetometry, while a detailed investigation of T_N was per-

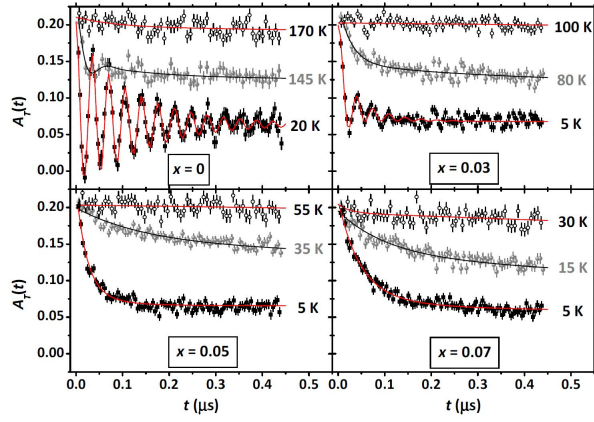


FIG. 1: (Color online) ZF μ^+ -depolarization curves for four $\text{CeFe}_{1-x}\text{Co}_x\text{AsO}$ samples ($0 \leq x \leq 0.07$) at representative T values. Continuous lines are best fits to experimental data according to the analysis described in the SM. Data for $x = 0$ are taken from Ref. [6].

formed by means of μ^+ SR [28]. The results of the characterizations as well as the precise information about the definitions of the critical temperatures T_N , T_c and T_N^{Ce} are reported in the SM.

Sets of experimental μ^+ spin-depolarization curves $A_T(t)$ in zero-magnetic field (ZF) at different temperatures (T) are shown in Fig. 1 for several $\text{CeFe}_{1-x}\text{Co}_x\text{AsO}$ samples ($0 \leq x \leq 0.07$). Data are analyzed as described in the SM. Two inequivalent crystallographic sites for μ^+ are observed in agreement with previous results on oxy-pnictides [29–31]. Because of the dipolar interaction between μ^+ and the antiferromagnetic FeAs layers, μ^+ are very sensitive to magnetic ordering even when the magnetic coherence length ξ_m is of the order of few nanometers. Typically, the precessions of μ^+ around the local magnetic fields are rapidly overdamped when $\xi_m \lesssim 10$ lattice constants [28, 32]. This is exactly the case of $\text{CeFe}_{1-x}\text{Co}_x\text{AsO}$ for $x \gtrsim 0.035$, as shown in Fig. 1, a result indicating that the long-range magnetic order (LRO) realized at $x = 0$, where $\xi_m \gg 1$ nm, is gradually driven to a short-range magnetic order (SRO), where $\xi_m \sim 1$ nm for higher x concentrations.

The full electronic phase diagram of $\text{CeFe}_{1-x}\text{Co}_x\text{AsO}$ is presented in Fig. 2. By comparing these results with what is reported for $\text{CeFeAsO}_{1-x}\text{F}_x$ [6], it is immediately clear that the SC properties are affected differently by the two chemical dilutions. In particular, the typical values $T_c \simeq 10$ K for $\text{CeFe}_{1-x}\text{Co}_x\text{AsO}$ at optimal doping are much lower than what is observed for $\text{CeFeAsO}_{1-x}\text{F}_x$, namely $T_c \simeq 35$ K [6, 10, 16]. This suggests that the $\text{Fe}_{1-x}\text{Co}_x$ dilution is generally detrimental to SC since it introduces a sizeable degree of disorder directly on the active FeAs layers. However, the region of coexistence between SDW and SC phases is similar to what was reported for $\text{SmFeAsO}_{1-x}\text{F}_x$ and $\text{CeFeAsO}_{1-x}\text{F}_x$ [4–6]. In

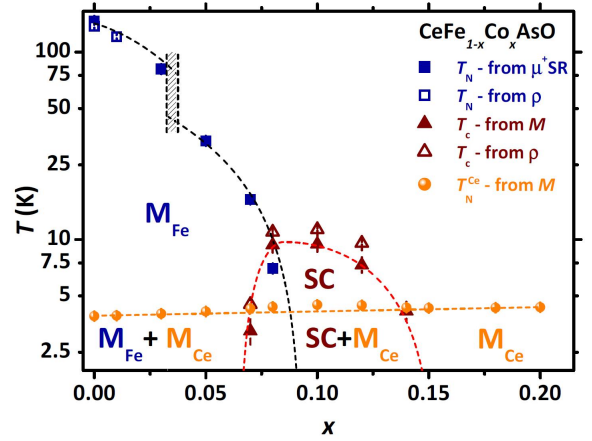


FIG. 2: (Color online) Electronic phase diagram for $\text{CeFe}_{1-x}\text{Co}_x\text{AsO}$. M_{Fe} and M_{Ce} refer to magnetic phases of Fe and Ce, respectively. The dashed lines are empirical guides for the eyes. Dashed lines on the magnetic side of the phase diagram are discussed in more detail in Fig. 3.

particular, an extremely narrow coexistence region for the two electronic ground states is observed for both the in-plane and out-of-plane substitutions in the 1111 family. Under these conditions, 100% of the sample volume is magnetic while, at the same time, a sizeable bulk region displays SC (see SM). From these arguments, a segregation of the two phases at the nanoscopic level was deduced in $\text{SmFeAsO}_{1-x}\text{F}_x$ and $\text{CeFeAsO}_{1-x}\text{F}_x$ and the same scenario holds also in the case of $\text{Fe}_{1-x}\text{Co}_x$ dilution. This scenario is completely different from what is detected in La-based 1111 materials [2, 33, 34]. It should be stressed that such nanoscopic coexistence is detected in $\text{CeFeAsO}_{1-x}\text{F}_x$ and $\text{CeFe}_{1-x}\text{Co}_x\text{AsO}$ only when the magnetic phase is short-ranged. Remarkably, this is qualitatively different from what is obtained in the electron-doped 122 materials like $\text{Ba}(\text{Fe}_{1-x}\text{Co}_x)_2\text{As}_2$, where the x -range of coexistence is typically much wider [11, 35], superconductivity being reported to emerge still in the presence of clear coherent oscillations for the SDW phase [36]. The appearance of superconductivity even in the presence of a LRO magnetic phase is possibly a fingerprint of the 122 family, at variance with what is generally observed in 1111 materials. This can be observed by comparing the results presented in Ref. [36] with what is reported in the case of hole-doping realized by means of the $\text{Ba}_{1-x}\text{K}_x$ substitution [37].

With the aim to precisely compare the effects of the in-plane and out-of-plane dilutions in CeFeAsO , the values of T_N versus x in $\text{CeFe}_{1-x}\text{Co}_x\text{AsO}$ are reported in the main panel of Fig. 3, together with data for $\text{CeFeAsO}_{1-x}\text{F}_x$, the latter being taken from Ref. [6]. It should be stressed that x concentrations for the latter materials should be considered as real after an *a posteriori* determination by means of nuclear magnetic reso-

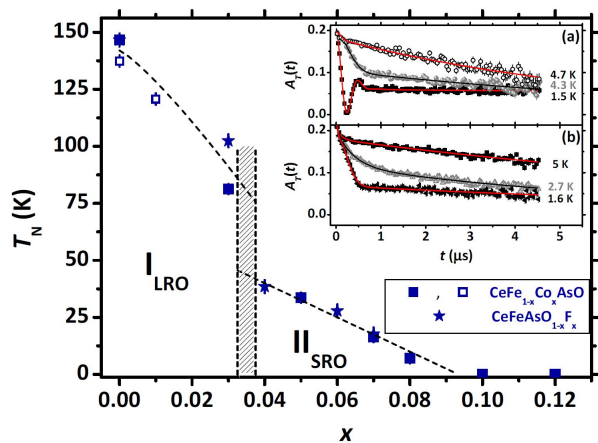


FIG. 3: (Color online) Main panel: T_N versus x for Co- and F-doped CeFeAsO (the latter data are taken from Ref. [6]). Close and open symbols refer to estimates from μ^+ SR and resistivity, respectively. The shaded region indicates the crossover between the LRO and SRO magnetic regimes. The dashed lines are empirical guides for the eyes. Inset: comparison between ZF μ^+ -depolarization curves at representative T for samples in the SC region of the phase diagram for both CeFe $_{1-x}$ Co $_x$ AsO ($x = 0.12$), panel (a), and CeFeAsO $_{1-x}$ F $_x$ ($x = 0.08$), panel (b). Continuous lines are best fits to experimental data according to the analysis described in SM.

nance [6]. Remarkably, results for both the families of compounds display a common behavior. Magnetism is indeed driven only by the amount of dilution regardless of the possible different modifications both of the details of the band structure or of the introduced degree of in-plane disorder. Two qualitatively different trends for the suppression of T_N with increasing x can be detected, which are associated with LRO and SRO (denoted as I_{LRO} and II_{SRO} in Fig. 3, respectively). In particular, a linear dependence of T_N on x common to both F- and Co-diluted compounds is encountered in the intermediate-doping region close to the appearance of SC. The results are similar to what is realized in Fe $_{1+y}$ Se $_x$ Te $_{1-x}$, where the region II is associated with the emergence of a glassy-like magnetism [38, 39]. Remarkably, the phase diagram is also highly reminiscent of hole-doped cuprates, such as La $_{2-x}$ Sr $_x$ CuO $_4$ and Y $_{1-x}$ Ca $_x$ Ba $_2$ Cu $_3$ O $_{6+y}$, where the glassy magnetism is also generally reported to be fully suppressed for $x \sim 0.1$ [40, 41]. However, the coherent oscillations of the μ^+ SR signal are clearly detected also well-inside region II both for Fe $_{1+y}$ Se $_x$ Te $_{1-x}$ and for the cuprates due to clusters whose magnetic moment freezes at low T [39, 41]. This inhomogeneous magnetic order is often referred to as cluster spin glass.

In spite of the above similarities, clear qualitative differences among the effects of in-plane and out-of-plane disorders are enlightened concerning the features of the magnetic phase of the Ce sublattice. As reported in Refs. [6] and [10], T_N^{Ce} is strongly suppressed in

CeFeAsO $_{1-x}$ F $_x$ as x increases and eventually vanishes in correspondence with the full suppression of the SDW phase. A similar phenomenology was recently reported in CeFe $_{1-x}$ Ru $_x$ AsO even though a much weaker dependence on x was detected in this case [42]. This would suggest that the two magnetic phases are intimately connected and that the ordering of the Ce sublattice is induced by the molecular field generated by the SDW [10]. The current results clarify that this is not really the case, since data for CeFe $_{1-x}$ Co $_x$ AsO unambiguously show that the magnetic phase of the Ce sublattice is still present at $x = 0.2$, although the SDW is fully suppressed already at $x = 0.1$ (see Figs. 2 and 3). Similar results were recently reported also in the case of isovalent dilution in CeFeAs $_{1-x}$ P $_x$ O [43]. This observation for samples well inside the SC phase is in agreement with what is reported in Ref. [16] and it is here reinforced by μ^+ SR data (see Fig. 3, inset). One clearly detects coherent oscillations in the case of CeFe $_{0.88}$ Co $_{0.12}$ AsO indicative of a long-range ordered phase, even though the transverse damping is quite severe ($\lambda_1^{\text{Tr}} \simeq 4 \mu\text{s}$), see Fig. 3(a). On the other hand, in CeFeAsO $_{0.92}$ F $_{0.08}$ (nominal composition) the ordering of Ce $^{3+}$ ions can be detected from a qualitative change in the damping of the transverse relaxation, which from Lorentzian turns into a markedly Gaussian shape at the lowest T value, see Fig. 3(b). No clear signs of coherent oscillations can be distinguished in this case, again confirming that the O $_{1-x}$ F $_x$ dilution strongly affects the magnetic phase of the Ce $^{3+}$ ions.

These results can be interpreted in the light of two different mechanisms contributing to the magnetic coupling among Ce $^+$ ions, one of direct nature (e.g., superexchange via O $^{2-}$) and the other of indirect RKKY-like nature, via carriers belonging to the FeAs layers [44, 45]. The strong sensitivity of T_N^{Ce} to the local perturbation realized by the O $_{1-x}$ F $_x$ dilution shows that the former mechanism has the strongest impact to the overall magnetic coupling. Naively, this is favored by the spatial extension of the Ce $^{3+}$ electronic orbitals, typically larger than those of other rare-earth ions. The sizeable sensitivity of the direct term to the increasing F content completely hinders the modification of the RKKY interaction realized by the variation of the charge density on the FeAs bands and of the relative band structure. On the other hand, the in-plane Fe $_{1-x}$ Co $_x$ dilution does not affect the CeO layers locally and the main modification is expected to involve the indirect term. Moreover, the change of the extent of the $f-d$ hybridization among Ce $^{3+}$ ions and FeAs bands, triggered by the reduction of the volume of the crystallographic cell with increasing x [16], should also be considered. In this respect, it should be noticed that the gradual increase of T_N^{Ce} upon increasing x in CeFe $_{1-x}$ Co $_x$ AsO (see the dashed straight line in Fig. 4) is in qualitative agreement with the similar trend observed after μ^+ SR measurements in undoped CeFeAsO under applied hydrostatic pressure [30]. These

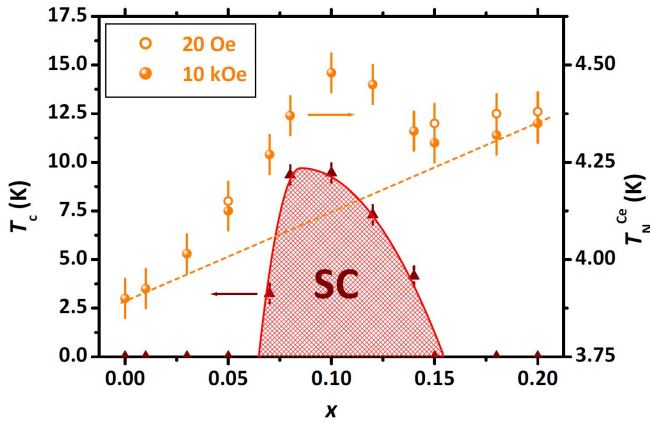


FIG. 4: (Color online) Main panel: T_c values as reported after measurements of dc magnetometry. T_N^{Ce} is also plotted (on a different scale) for two different values of magnetic field. The continuous and dashed lines are empirical guides for the eyes.

results deserve a more detailed computational investigation in order to precisely unveil the details of such complex interplay of subtle many-body effects.

Quite surprisingly, the magnetic coupling among Ce^{3+} ions is anomalously enhanced in the presence of SC. This is clearly evidenced in Fig. 4, where a dome-like behaviour for T_N^{Ce} versus x in correspondence with the emergence of the SC dome is superimposed to the overall linear increase described above. T_N^{Ce} deduced by means of dc magnetometry is known to be strongly suppressed as the value of the measuring field increases for typical values $H \gtrsim 10$ kOe (see SM). At first sight, the enhancement of T_N^{Ce} could be associated with the shielding of the external field by the SC-induced supercurrents. This effect would apparently increase the critical temperature itself. However, this scenario is ruled out by the tiny discrepancy observed among measurements at $H = 20$ Oe and 10 kOe, thus implying that the applied H field value cannot be at the origin of the observed T_N^{Ce} suppression. The explanation possibly relies on the modification of the indirect RKKY coupling through the involvement of FeAs bands into SC. Still, the results are even more intriguing in view of the possible occurrence of subtle many-body effects like the Kondo screening and its interplay with SC. This issue has been discussed in the literature from a theoretical point of view, showing how a competition between these two mechanisms is at work in oxy-pnictides [46]. Our results display a common enhancement of Ce magnetism and SC and are not in contrast with such theoretical scenario.

Summarizing, in this Letter we discussed the effects of the in-plane and out-of-plane chemical substitutions in CeFeAsO realized by $\text{Fe}_{1-x}\text{Co}_x$ and O_{1-x}F_x dilutions, respectively. Remarkably, $\mu^+\text{SR}$ enlightened that the spin-density-wave phase is suppressed in a quantitatively

identical fashion in both cases, showing that the degree of the in-plane disorder is not playing any substantial role. At variance with the behavior for the spin-density-wave, such in-plane disorder strongly affects the superconducting properties resulting in a much more effective suppression of T_c for the $\text{Fe}_{1-x}\text{Co}_x$ rather than for the O_{1-x}F_x dilution. The unusual behavior of Ce magnetism was discussed in the light of the different kinds of disorder introduced by the two considered chemical substitutions. Our surprising results clearly deserve a more detailed computational investigation concerning the precise role of indirect RKKY-like coupling among the localized Ce^{3+} magnetic moments, also in relation with the anomalous enhancement of the ordering temperature T_N^{Ce} in the presence of superconductivity.

G. Prando acknowledges support from the Leibniz-Deutscher Akademischer Austauschdienst (DAAD) Post-Doc Fellowship Program and stimulating discussions with A. Akbari, J. Geck and P. Thalmeier. S. Sanna and P. Carretta acknowledge support from Fondazione Cariplo (research grant No. 2011-0266). G. Lamura acknowledges support from the FP7 European project SUPER-IRON (grant agreement no. 283204). S. Wurmehl acknowledges support by the Deutsche Forschungsgemeinschaft DFG under the Emmy-Noether programme (grant no. WU595/3-1). This work has been supported by the Deutsche Forschungsgemeinschaft DFG through the Priority Programme SPP1458 (grants no. BE1749/13 and no. GR3330/2) and the Graduate School GRK 1621.

SUPPLEMENTAL MATERIAL

Synthesis of samples

Polycrystalline samples of $\text{CeFe}_{1-x}\text{Co}_x\text{AsO}$ ($0 \leq x \leq 0.2$) have been prepared by a two-step solid-state reaction similarly to what is described in Ref. [47]. In the first step, CeAs was prepared from Ce slugs (Chempur, 99.9%) and As lumps (Alfa Aesar, 99.999%) reacting a stoichiometric ratio in an evacuated quartz tube placed in a two-zone furnace. In the second step, we used the resulting CeAs and mixed it with Fe (Alfa Aesar, 99.998%), Fe_2O_3 (Chempur, 99.999%), and Co (Goodfellow, 99.99%) in a stoichiometric ratio. All starting materials were homogenized by grinding in a ball mill. The resulting powders were pressed into pellets under Ar atmosphere using a pressure of 20 kN, and subsequently annealed in an evacuated quartz tube in a two-step annealing process at 940°C for 8 h and at 1150°C for 48 h.

In order to confirm the single-phase character of the polycrystals, powder x-ray diffraction was performed on a Huber Guinier camera (Co K_α radiation). The samples were either pure or contained small amounts of CeAs,

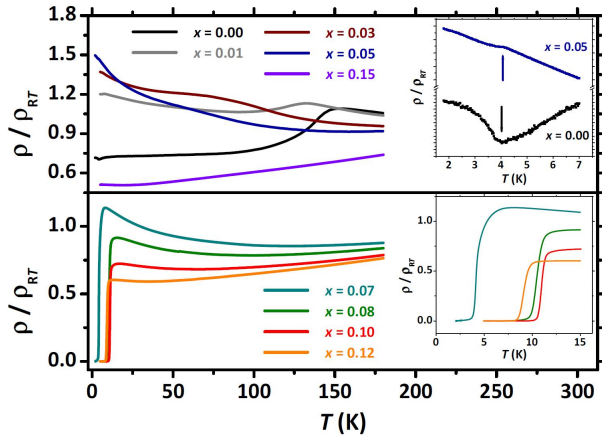


FIG. 5: (Color online) ρ versus T for $\text{CeFe}_{1-x}\text{Co}_x\text{AsO}$ samples in ZF conditions. Data for non-SC and SC samples are plotted in the upper and lower panels, respectively. Upper inset: enlargement of data for non-SC samples displaying kinks at T_N^{Ce} (see arrow - different scales are used for the two samples). Lower inset: enlargement of data for SC samples in the low- T region.

Co_3O_4 , Fe_3O_4 and/or FeAs . The microstructure and the composition were examined by scanning electron microscopy (XL30 Philipps, IN400) equipped with an electron microprobe analyzer for semi-quantitative elemental analysis using the wavelength dispersive x-ray mode. The analysis showed a good agreement between the nominal and the measured Co contents. Accordingly, the nominal content is used to label the samples.

Characterization of samples

Electrical transport

Measurements of electrical resistivity (ρ) were performed in conditions of zero-magnetic field (ZF) as a function of temperature (T) by means of a standard four-probe setup. The T -dependence of ρ for $\text{CeFe}_{1-x}\text{Co}_x\text{AsO}$ samples ($0 \leq x \leq 0.15$) is shown in Fig. 5. The curves are normalized with respect to the relative ρ_{RT} values at room T (RT) for a better visualization of data. In the case of CeFeAsO , the pronounced maximum at around 150 K and the inflection point at slightly lower T can be related to the critical temperatures for the structural and spin-density-wave (SDW) transitions, T_s and T_N respectively [10, 27]. These anomalies can be discerned up to $x = 0.03$ even if a sizeable and progressive broadening prevents one from a precise definition of T_s and T_N for $x > 0.01$. However, a progressive suppression of both T_s and T_N with increasing x can be inferred as a clear trend, in agreement with data reported in the literature [16]. The clear kinks in ρ versus T curves at $T \simeq 4$ K are associated to the magnetic ordering temperature T_N^{Ce} for

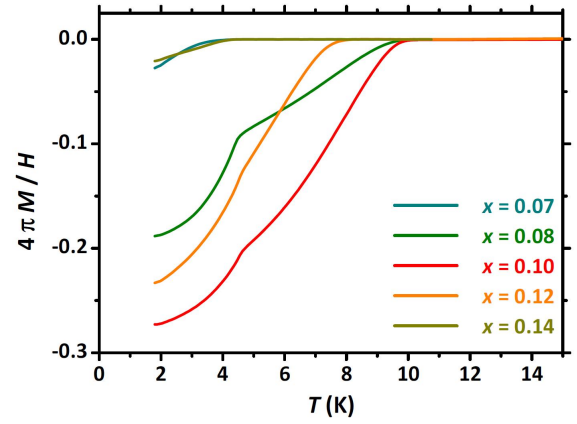


FIG. 6: (Color online) dc susceptibility for $\text{CeFe}_{1-x}\text{Co}_x\text{AsO}$ SC samples. Measurements were performed at $H = 20$ Oe in ZF-cooled conditions. The clear kinks at $T \simeq 4$ K are associated with T_N^{Ce} (see also Fig. 7).

the Ce sublattice (see the upper inset of Fig. 5). A further increase in the level of Co-doping ($0.07 \leq x \leq 0.12$) leads to the appearance of superconductivity (SC) with the highest value for the critical temperature T_c being realized for the optimal-doping value $x \simeq 0.1$ (see the inset in the lower panel of Fig. 5) while SC is fully suppressed by increasing the Co doping to values $x \geq 0.15$. Our data are in good agreement with early reports in the literature [14–16].

dc magnetometry

The magnetic characterization of the samples was performed by means of a MPMS-XL5 SQUID dc magnetometer (Quantum Design). Results for the SC materials are presented in Fig. 6 where a dome-like behaviour for the critical temperature T_c for the SC phase is evident. The maximum shielding fraction can be roughly estimated as 30%, in good agreement with previous reports on F-doped CeFeAsO [6, 32] even if systematically lower values are found in the current case (no demagnetization effects from the geometrical shape of the grains were considered at all). However, the picture is very useful in order to check that the SC phase is not filamentary in the considered materials even if a precise estimate of the SC fraction can not be obtained from the current data.

The value of T_N^{Ce} can be clearly detected by means of dc magnetometry since magnetization M displays sharp peaks in correspondence to those critical temperatures (see figs. 6 and 7). A strong dependence of such quantity on the external magnetic field is detected as shown in the main panel of Fig. 7. However, it should be remarked that in the limit $H \lesssim 10$ kOe the results display an almost negligible dependence of T_N^{Ce} on H (see the in-

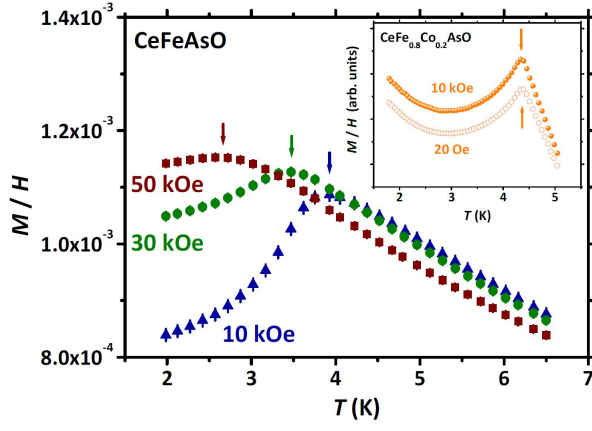


FIG. 7: (Color online) Main panel: dc susceptibility for CeFeAsO in the high- H regime. The arrows indicate T_N^{Ce} . Inset: dc susceptibility for CeFe_{0.8}Co_{0.2}AsO in the low- H regime.

set of Fig. 7). The error bars associated to results for SC samples at low- H values are by far too big if compared to what is obtained for non-SC materials (see Fig. 6).

Muon spin spectroscopy

In a μ^+ SR experiment, a spin-polarized beam of positive muons μ^+ is implanted into the investigated sample. Coulomb scattering processes typically lead to the thermalization of μ^+ at interstitial crystallographic sites without the loss of spin polarization. After a mean life time $\tau_{\mu^+} \simeq 2.17\mu\text{s}$, every μ^+ decays emitting a positron e^+ with linear momentum preferentially parallel to the direction of the spin of the μ^+ at the instant of the decay. As a consequence, a spatially-resolved detection of e^+ as a function of time (t) allows one to probe magnetism on a local scale [28]. The typical output of a ZF- μ^+ SR experiment for magnetic materials is the depolarization function

$$\frac{A_T(t)}{A_0} = [1 - V_m(T)] e^{-\frac{\sigma_N^2 t^2}{2}} + \sum_{i=1}^N \zeta_i [a_i^{\text{Tr}}(T) F_i(t) D_i^{\text{Tr}}(t) + a_i^{\text{L}}(T) D_i^{\text{L}}(t)] \quad (1)$$

describing the t -dependence of the spin polarization of μ^+ at T . Here, A_0 is an instrument-dependent parameter corresponding to the condition of full spin polarization. In the paramagnetic phase of the investigated material, μ^+ are subject to nuclear magnetism leading to a slow Gaussian damping quantified by σ_N . In the presence of a magnetic phase, a fraction $V_m(T)$ of μ^+ probe a static local magnetic field and this quantity reflects the magnetic volume fraction of the sample at T , accordingly. The labels Tr and L in eq. (1) refer to μ^+ probing local

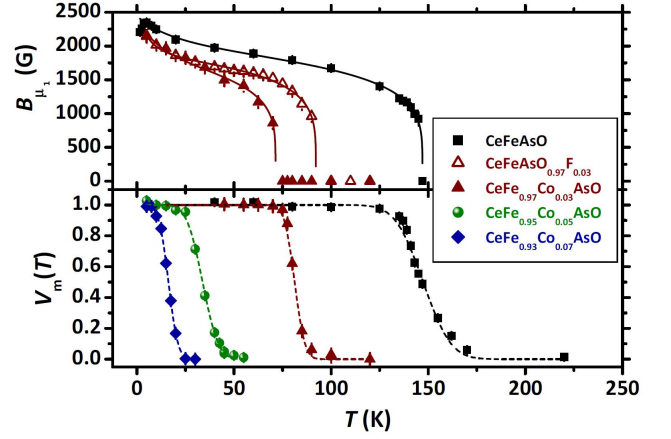


FIG. 8: (Color online) Upper panel: T -dependence of the internal field at the μ^+ site B_{μ_1} for $x = 0$ and $x = 0.03$ (both F- and Co-dilutions are considered). The continuous lines are best-fits to data according to eq. (2). Lower panel: T -dependence of the magnetic volume fraction $V_m(T)$ for the CeFe_{1-x}Co_xAsO samples ($x \leq 0.07$). The dashed lines are best-fits to data according to eq. (3).

magnetic fields B_μ in transverse or longitudinal directions with respect to the initial spin polarization, respectively. $F(t)$ oscillating functions represent the precession of μ^+ around the local field B_μ while $D^{\text{Tr,L}}(t)$ quantify the damping of the signal. $D^{\text{Tr}}(t)$ is typically associated with the static distribution of local magnetic fields while $D^{\text{L}}(t)$ probes $1/T_1$ -like dynamical processes. The index i in eq. (1) allows for the possible presence of inequivalent crystallographic sites for μ^+ whose population is controlled by the parameters ζ_i such that $\sum_i \zeta_i = 1$.

Measurements of μ^+ SR were performed at μS (Paul Scherrer Institute, Switzerland) on both the GPS and Dolly low-background spectrometers at different temperatures (T) and in ZF conditions. The presence of two inequivalent crystallographic sites for μ^+ is envisaged ($i = 1, 2$) in agreement with previous results on oxy-pnictides [29–31]. In the current case of CeFe_{1-x}Co_xAsO, one finds $\zeta_1/\zeta_2 \simeq 4$ for the occupation probabilities of the sites ζ_i independently from the actual x value. The fitting results show that the magnetic volume fraction $V_m(T)$ associated with the SDW phase is maintained at around 100% in the low- T saturation limit independently from x (see Fig. 8, lower panel). μ^+ implanted at site 1 probe long-range magnetism in CeFeAsO as clearly seen by the long-lived coherent oscillation in the Tr component. In particular, the function $F_1(t) = \cos(\gamma_\mu B_{\mu_1} t)$ describes well the data while $F_1(t) = J_0(\gamma_\mu B_{\mu_1} t)$ is needed in order to reproduce the experimental trend for $x = 0.03$ (J_0 standing for a zeroth-order first-kind Bessel function and γ_μ being the gyromagnetic ratio for μ^+). This is a well-known result for oxy-pnictide materials and it hints at the gradual modification of the SDW phase from commensurability

to incommensurability with the underlying lattice upon increasing the charge doping while at the same time reducing the nesting of the Fermi surface [25, 48]. The results for B_{μ_1} as a function of T are displayed in the upper panel of Fig. 8. In the same figure, it is shown how the phenomenological function

$$B_{\mu_1}(T) = B_{\mu_1}^{\text{sat}} \left[1 - \left(\frac{T}{T_N} \right)^\alpha \right]^\beta \left(1 + \frac{C_{\text{CW}}}{T - \theta} \right) \quad (2)$$

first proposed in Ref. [29] correctly reproduce the experimental data also in the case of the Co-doped $x = 0.03$ sample. In particular, the first term on the right side of eq. (2) accounts for a double-exponent power-law-like behaviour of the internal field due to the magnetic ordering of Fe while the second term accounts for a feedback paramagnetic polarization of the Ce sublattice induced by the molecular field of Fe and governed by the Curie-Weiss constant C_{CW} and the Curie-Weiss temperature θ [29]. In the fitting procedure for all the three samples, the values $\alpha = 2.1$ and $\beta = 0.2$ have been kept fixed in order to reduce the number of free parameters (the values have been extracted from what is reported in the literature [29]).

The gradual disordering of the magnetic phase leads to the disappearance of oscillations in the Tr component for $x \geq 0.05$, $F_1(t)$ being overdamped by a sizeable distribution of static local magnetic fields. This corresponds to $F_1(t) = 1$ for both $x = 0.05$ and 0.07 samples with transversal dampings described as $D_1^{\text{Tr}}(t) = \exp(-\lambda_1^{\text{Tr}} t)$. At the lowest investigated temperature ($T = 5$ K), one has $\lambda_1^{\text{Tr}} \simeq 45 \mu\text{s}$ and $25 \mu\text{s}$ for $x = 0.05$ and 0.07 , respectively. Such values are quite typical in the region of coexistence between magnetism and SC for oxypnictides [6, 32]. On the other hand, μ^+ implanted at site 2 probe sizeable distributions of local magnetic fields for all the samples and $F_2(t) = 1$, accordingly, with $D_2^{\text{Tr}}(t) = \exp(-\lambda_2^{\text{Tr}} t)$. At $T = 5$ K, one has $\lambda_2^{\text{Tr}} \simeq 25 \mu\text{s}$, $20 \mu\text{s}$, $15 \mu\text{s}$ and $8 \mu\text{s}$ for $x = 0, 0.03, 0.05$ and 0.07 , respectively.

T_N is precisely quantified from the actual T -dependence of the magnetic volume fraction $V_m(T)$ after a fitting procedure according to the error-function-like expression [6, 30, 32]

$$V_m(T) = \frac{1}{2} \operatorname{erfc} \left[\frac{T - T_N}{\sqrt{2}\Delta} \right] \quad (3)$$

where the complementary error function $\operatorname{erfc}(x)$ is defined as

$$\operatorname{erfc}(x) = \frac{2}{\sqrt{\pi}} \int_x^{+\infty} e^{-t^2} dt. \quad (4)$$

In particular, T_N turns out to be defined as the T value corresponding to 50% of the magnetic volume fraction.

* E-mail: g.prando@ifw-dresden.de

- [1] Y. Kamihara, T. Watanabe, M. Hirano, H. Hosono, *Journ. Am. Chem. Soc.* **130**, 3296 (2008)
- [2] H. Luetkens, H.-H. Klauss, M. Kraken, F. J. Litterst, T. Dellmann, R. Klingeler, C. Hess, R. Khasanov, A. Amato, C. Baines, M. Kosmala, O. J. Schumann, M. Braden, J. Hamann-Borrero, N. Leps, A. Kondrat, G. Behr, J. Werner, B. Büchner, *Nature Mat.* **8**, 305 (2009)
- [3] J. Zhao, Q. Huang, C. de la Cruz, S. Li, J. W. Lynn, Y. Chen, M. A. Green, G. F. Chen, G. Li, Z. Li, J. L. Luo, N. L. Wang, P. Dai, *Nature Mat.* **7**, 953 (2008)
- [4] A. J. Drew, C. Niedermayer, P. J. Baker, F. L. Pratt, S. J. Blundell, T. Lancaster, R. H. Liu, G. Wu, X. H. Chen, I. Watanabe, V. K. Malik, A. Dubroka, M. Rössle, K. W. Kim, C. Baines, C. Bernhard, *Nature Mat.* **8**, 310 (2009)
- [5] S. Sanna, R. De Renzi, G. Lamura, C. Ferdeghini, A. Palenzona, M. Putti, M. Tropeano, and T. Shiroka, *Phys. Rev. B* **80**, 052503 (2009)
- [6] T. Shiroka, G. Lamura, S. Sanna, G. Prando, R. De Renzi, M. Tropeano, M. R. Cimberle, A. Martinelli, C. Bernini, A. Palenzona, R. Fittipaldi, A. Vecchione, P. Carretta, A. S. Siri, C. Ferdeghini, and M. Putti, *Phys. Rev. B* **84**, 195123 (2011)
- [7] Z.-A. Ren, W. Lu, J. Yang, W. Yi, X.-L. Shen, Z.-C. Li, G.-C. Che, X.-L. Dong, L.-L. Sun, F. Zhou, and Z.-X. Zhao, *Chin. Phys. Lett.* **25**, 2215 (2008)
- [8] D. C. Johnston, *Adv. Phys.* **59**, 803 (2010)
- [9] G. Prando, A. Lascialfari, A. Rigamonti, L. Romanó, S. Sanna, M. Putti, and M. Tropeano, *Phys. Rev. B* **84**, 064507 (2011)
- [10] H. Maeter, J. E. Hamann-Borrero, T. Goltz, J. Spehling, A. Kwadrin, A. Kondrat, L. Veyrat, G. Lang, H.-J. Grafe, C. Hess, G. Behr, B. Büchner, H. Luetkens, C. Baines, A. Amato, N. Leps, R. Klingeler, R. Feyerherm, D. Argyriou, and H.-H. Klauss, arXiv:1210.6959 (2012)
- [11] N. Ni, A. Thaler, J. Q. Yan, A. Kracher, E. Colombier, S. L. Bud'ko, P. C. Canfield, and S. T. Hannahs, *Phys. Rev. B* **82**, 024519 (2010)
- [12] M. A. Tanatar, N. Ni, A. Thaler, S. L. Bud'ko, P. C. Canfield, and R. Prozorov, *Phys. Rev. B* **84**, 014519 (2011)
- [13] A. S. Sefat, A. Huq, M. A. McGuire, R. Jin, B. C. Sales, D. Mandrus, L. M. D. Cranswick, P. W. Stephens, and K. H. Stone, *Phys. Rev. B* **78**, 104505 (2008)
- [14] J. Prakash, S. J. Singh, S. Patnaik, and A. K. Ganguli, *Solid State Commun.* **149**, 181 (2009)
- [15] L.-D. Zhao, D. Berardan, C. Byl, L. Pinsard-Gaudart, and N. Dragoe, *J. Phys.: Condens. Matter* **22**, 115701 (2010)
- [16] T. Shang, L. Yang, Y. Chen, N. Cornell, F. Ronning, J. L. Zhang, L. Jiao, Y. H. Chen, J. Chen, A. Howard, J. Dai, J. D. Thompson, A. Zakhidov, M. B. Salamon, and H. Q. Yuan, *Phys. Rev. B* **87**, 075148 (2013)
- [17] A. S. Sefat, R. Jin, M. A. McGuire, B. C. Sales, D. J. Singh, and D. Mandrus, *Phys. Rev. Lett.* **101**, 117004 (2008)
- [18] A. Yamamoto, J. Jaroszynski, C. Tarantini, L. Balicas, J. Jiang, A. Gurevich, D. C. Larbalestier, R. Jin, A. S. Sefat, M. A. McGuire, B. C. Sales, D. K. Christen, D. Mandrus, *Appl. Phys. Lett.* **94**, 062511 (2009)
- [19] H. Wadati, I. Elfimov, and G. A. Sawatzky, *Phys. Rev. Lett.* **105**, 157004 (2010)

- [20] T. Berlijn, C.-H. Lin, W. Garber, and W. Ku, *Phys. Rev. Lett.* **108**, 207003 (2012)
- [21] E. M. Bittar, C. Adriano, T. M. Garitezi, P. F. S. Rosa, L. Mendonça-Ferreira, F. Garcia, G. de M. Azevedo, P. G. Pagliuso, and E. Granado, *Phys. Rev. Lett.* **107**, 267402 (2011)
- [22] M. Merz, F. Eilers, T. Wolf, P. Nagel, H. v. Löhneysen, and S. Schuppler, *Phys. Rev. B* **86**, 104503 (2012)
- [23] G. Levy, R. Sutarto, D. Chevrier, T. Regier, R. Blyth, J. Geck, S. Wurmehl, L. Harnagea, H. Wadati, T. Mizokawa, I. S. Elfimov, A. Damascelli, and G. A. Sawatzky, *Phys. Rev. Lett.* **109**, 077001 (2012)
- [24] P. Bonfà, P. Carretta, S. Sanna, G. Lamura, G. Prando, A. Martinelli, A. Palenzona, M. Tropeano, M. Putti, and R. De Renzi, *Phys. Rev. B* **85**, 054518 (2012)
- [25] C. Liu, G. D. Samolyuk, Y. Lee, N. Ni, T. Kondo, A. F. Santander-Syro, S. L. Bud'ko, J. L. McClesney, E. Rotenberg, T. Valla, A. V. Fedorov, P. C. Canfield, B. N. Harmon, and A. Kaminski, *Phys. Rev. Lett.* **101**, 177005 (2008)
- [26] R. M. Fernandes, M. G. Vavilov, and A. V. Chubukov, *Phys. Rev. B* **85**, 140512 (2012)
- [27] C. Hess, A. Kondrat, A. Narduzzo, J. E. Hamann-Borrero, R. Klingeler, J. Werner, G. Behr, and B. Büchner, *Europhys. Lett.* **87**, 17005 (2009)
- [28] A. Yaouanc and P. Dalmass de Réotier, *Muon Spin Rotation, Relaxation, and Resonance: Applications to Condensed Matter*, Oxford University Press, Oxford (2011)
- [29] H. Maeter, H. Luetkens, Y. G. Pashkevich, A. Kwadrin, R. Khasanov, A. Amato, A. A. Gusev, K. V. Lamonova, D. A. Chervinskii, R. Klingeler, C. Hess, G. Behr, B. Büchner, and H.-H. Klauss, *Phys. Rev. B* **80**, 094524 (2009)
- [30] R. De Renzi, P. Bonfà, M. Mazzani, S. Sanna, G. Prando, P. Carretta, R. Khasanov, A. Amato, H. Luetkens, M. Bendele, F. Bernardini, S. Massidda, A. Palenzona, M. Tropeano, and M. Vignolo, *Supercond. Sci. Technol.* **25**, 084009 (2012)
- [31] G. Prando, P. Bonfà, G. Profeta, R. Khasanov, F. Bernardini, M. Mazzani, E. M. Brünig, A. Pal, V. P. S. Awana, H.-J. Grafe, B. Büchner, R. De Renzi, P. Carretta, and S. Sanna, *Phys. Rev. B* **87**, 064401 (2013)
- [32] S. Sanna, R. De Renzi, T. Shiroka, G. Lamura, G. Prando, P. Carretta, M. Putti, A. Martinelli, M. R. Cimeterle, M. Tropeano, and A. Palenzona, *Phys. Rev. B* **82**, 060508 (2010)
- [33] R. Khasanov, S. Sanna, G. Prando, Z. Shermadini, M. Bendele, A. Amato, P. Carretta, R. De Renzi, J. Karpinski, S. Katrych, H. Luetkens, and N. D. Zhigadlo, *Phys. Rev. B* **84**, 100501 (2011)
- [34] G. Prando, S. Sanna, G. Lamura, T. Shiroka, M. Tropeano, A. Palenzona, H.-J. Grafe, B. Büchner, P. Carretta, and R. De Renzi, *Phys. Stat. Sol. B* **250**, 599 (2013)
- [35] R. M. Fernandes, D. K. Pratt, W. Tian, J. Zarestky, A. Kreyssig, S. Nandi, M. G. Kim, A. Thaler, N. Ni, P. C. Canfield, R. J. McQueeney, J. Schmalian, and A. I. Goldman, *Phys. Rev. B* **81**, 140501 (2010)
- [36] C. Bernhard, C. N. Wang, L. Nuccio, L. Schulz, O. Zaharko, J. Larsen, C. Aristizabal, M. Willis, A. J. Drew, G. D. Varma, T. Wolf, and C. Niedermayer, *Phys. Rev. B* **86**, 184509 (2012)
- [37] E. Wiesenmayer, H. Luetkens, G. Pascua, R. Khasanov, A. Amato, H. Potts, B. Banusch, H.-H. Klauss, and D. Johrendt, *Phys. Rev. Lett.* **107**, 237001 (2011)
- [38] N. Katayama, S. Ji, D. Louca, S.-H. Lee, M. Fujita, T. J. Sato, J. S. Wen, Z. J. Xu, G. D. Gu, G. Xu, Z. W. Lin, M. Enoki, S. Chang, K. Yamada, and J. M. Tranquada, *Journ. Phys. Soc. Jpn.* **79**, 113702 (2010)
- [39] G. Lamura, T. Shiroka, P. Bonfà, S. Sanna, F. Bernardini, R. De Renzi, R. Viennois, E. Giannini, A. Piriou, N. Emery, M. Cimeterle, and M. Putti, *J. Phys.: Condens. Matter* **25**, 156004 (2013)
- [40] M.-H. Julien, *Physica B* **329-333**, 693 (2003) and references therein
- [41] S. Sanna, F. Coneri, A. Rigoldi, G. Concas, S. R. Giblin, and R. De Renzi, *Phys. Rev. B* **82**, 100503 (2010)
- [42] C. Wang, H. Jiang, Y. Luo, C. Feng, W. Li, Z. Xu, G. Cao, J. H. Kim, and S. Dou, *Europhys. Lett.* **99**, 57009 (2012)
- [43] A. Jesche, T. Förster, J. Spehling, M. Nicklas, M. de Souza, R. Gumeniuk, H. Luetkens, T. Goltz, C. Krellner, M. Lang, J. Sichelschmidt, H.-H. Klauss, and C. Geibel, *Phys. Rev. B* **86**, 020501 (2012)
- [44] G. Prando, P. Carretta, A. Rigamonti, S. Sanna, A. Palenzona, M. Putti, and M. Tropeano, *Phys. Rev. B* **81**, 100508 (2010)
- [45] A. Akbari, P. Thalmeier, and I. Eremin, arXiv:1301.6497v1 (2013)
- [46] L. Pourovskii, V. Vildosola, S. Biermann, A. Georges, *Europhys. Lett.* **84**, 37006 (2008)
- [47] A. Kondrat, J. E. Hamann-Borrero, N. Leps, M. Kosmala, O. Schumann, A. Köhler, J. Werner, G. Behr, M. Braden, R. Klingeler, B. Büchner, and C. Hess, *Eur. Phys. J. B* **70**, 461 (2009)
- [48] J. P. Carlo, Y. J. Uemura, T. Goko, G. J. MacDougall, J. A. Rodriguez, W. Yu, G. M. Luke, P. Dai, N. Shannon, S. Miyasaka, S. Suzuki, S. Tajima, G. F. Chen, W. Z. Hu, J. L. Luo, N. L. Wang, *Phys. Rev. Lett.* **102**, 087001 (2008)